J. Fluid Mech. (2011), *vol.* 686, *pp.* 26–39. © Cambridge University Press 2011
doi:10.1017/jfm.2011.315

Suspensions in a tilted trough: second normal stress difference

Étienne Couturier, François Boyer†, Olivier Pouliquen and Élisabeth Guazzelli

IUSTI-CNRS UMR 6595, Polytech-Marseille, Aix-Marseille Université (U1), Technopôle de Château-Gombert, 13453 Marseille CEDEX 13, France

(Received 10 March 2011; revised 25 May 2011; accepted 18 July 2011; first published online 21 September 2011)

We measure the second normal-stress difference in suspensions of non-Brownian neutrally buoyant rigid spheres dispersed in a Newtonian fluid. We use a method inspired by Wineman & Pipkin (*Acta Mechanica*, vol. 2, 1966, pp. 104–115) and Tanner (*Trans. Soc. Rheol.*, vol. 14, 1970, pp. 483–507), which relies on the examination of the shape of the suspension free surface in a tilted trough flow. The second normal-stress difference is found to be negative and linear in shear stress. The ratio of the second normal-stress difference to shear stress increases with increasing volume fraction. A clear behavioural change exhibiting a strong (approximately linear) growth in the magnitude of this ratio with volume fraction is seen above a volume fraction of 0.22. By comparing our results with previous data obtained for the same batch of spheres by Boyer, Pouliquen & Guazzeli (*J. Fluid Mech.*, 2011, doi:10.1017/jfm.2011.272), the ratio of the first normal-stress difference to the shear stress is estimated and its magnitude is found to be very small.

Key words: particle/fluid flow, rheology, suspensions

1. Introduction

Despite several decades of active research, the rheology of suspensions is not fully deciphered even in the simplest case of non-Brownian neutrally buoyant rigid spheres dispersed in a Newtonian fluid. When suspensions are subjected to simple shear flow at very low Reynolds numbers (see figure 1), the linearity of the Stokes equations implies a linear relation between the shear stress $\tau = \Sigma_{xy}$ and the shear rate $\dot{\gamma}$ and therefore a quasi-Newtonian rheological relation $\tau = \eta_s \dot{\gamma}$. The effective suspension viscosity is given by $\eta_s(\phi) = \eta_f \times f(\phi)$ where η_f is the viscosity of the pure Newtonian fluid and $f(\phi)$ is a sole function of the volume fraction ϕ which diverges when approaching maximum packing fraction (see e.g. Stickel & Powell 2005). However, this quasi-Newtonian relation does not fully describe the suspension rheology as differences in normal stresses develop, i.e. normal stresses are no longer isotropic, in the non-dilute limit. As the suspension is incompressible, the pressure itself (i.e. the trace of the bulk suspension stress Σ) is of no rheological interest, and the two relevant quantities are the first and second normal-stress differences defined as $N_1 = \Sigma_{yy} - \Sigma_{xx}$ and $N_2 = \Sigma_{yy} - \Sigma_{zz}$ respectively (see e.g. Bird, Armstrong &

† Email address for correspondence: francois.boyer@polytech.univ-mrs.fr

https://doi.org/10.1017/jfm.2011.315 Published online by Cambridge University Press

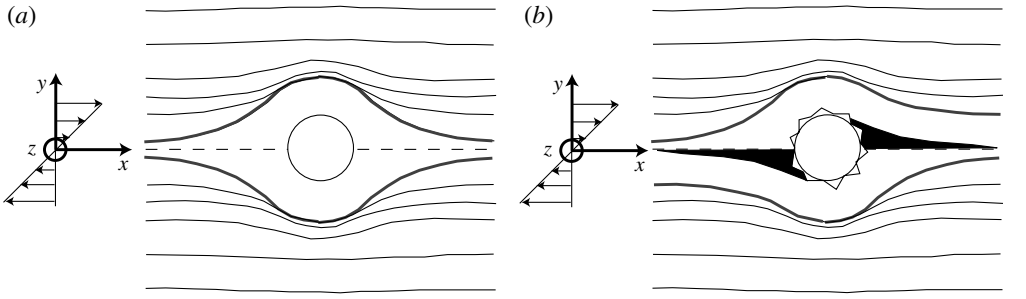


FIGURE 1. Sketch of the trajectories around a sphere subjected to a linear shear flow: (*a*) symmetry for perfectly smooth spheres and (*b*) asymmetry for rough spheres with depletion in the extensional quadrants indicated in black. The limiting (open) trajectories are indicated by thick lines.

Hassager 1987). As in viscoelastic fluids such as polymers, normal-stress differences in suspensions are of fundamental importance in many situations since they can induce secondary flows (Ramachandran & Leighton 2008) and instabilities (Brady & Carpen 2001). They are also related to flow-induced microstructure and, in particular, to particle migration (see e.g. Morris & Boulay 1999; Boyer *et al.* 2011). Again, for suspensions of non-Brownian hard spheres in the Stokes regime, dimensional analysis implies that N_1 and N_2 scale viscously as $\eta_f\dot{\gamma}$ and thus are proportional to the shear stress τ. It is useful to define the ratios of normal-stress differences to shear stress, $\alpha_1 = N_1/\tau$ and $\alpha_2 = N_2/\tau$, which are sole functions of ϕ and do not diverge at maximum packing fraction (see e.g. Morris & Boulay 1999; Zarraga, Hill & Leighton 2000).

Change in the suspension microstructure under shear is considered to be the fundamental ingredient for the development of the non-Newtonian features observed in suspensions (see e.g. Stickel & Powell 2005). Some understanding can be gained by considering solely pair interaction between particles under simple shear, as sketched in figure 1. For perfectly smooth spheres shown in figure 1(*a*), the motion is symmetric as it reflects the fore–aft symmetry of the flow lines around a single sphere due to the reversibility of the Stokes flow. Considering only Stokes flow regime, lubrication prevents the spheres from touching in a finite time. While this motion creates additional shear stress, it does not induce any normal stress differences as the effects of the compressive and extensive portions of the flow cancel (see e.g. Batchelor & Green 1972). Conversely, surface roughness (or repulsive force) makes collisions irreversible and asymmetric (Arp & Mason 1977; Davis 1992) and leads to the development of non-isotropic normal stresses (Brady & Morris 1997; Wilson 2005). Indeed, when the minimum approach distance for the pair is smaller than the roughness, the spheres come into contact in the compressional region of the flow and move apart in the extensional region, see figure 1(*b*). After the collision, the particles do not come back to their initial streamlines, but lie on two critical streamlines whose minimum approach distance is exactly the roughness. This results in a twofold origin of asymmetry. First, contact interactions only occur in the compressional region of the flow. Second, the breakdown of the fore–aft symmetry leads to weaker hydrodynamic interactions in the extensional region than in the compressional region due to the depletion in particles shown in black in figure 1(*b*). This fore–aft asymmetry has been observed both in experiments (Parsi & Gadala-Maria 1987; Rampall, Smart &

https://doi.org/10.1017/jfm.2011.315 Published online by Cambridge University Press

Leighton 1997) and in numerical simulations using Stokesian dynamics (Sierou & Brady 2002).

This rough sketch based on pair interactions is sufficient to explain the development of normal stress differences. The deficit in hydrodynamic interactions at the rear of the collision (i.e. in the extensional region) leads to a negative first normal stress difference $N_1 = \Sigma_{xx} - \Sigma_{yy}$. The second normal stress difference $N_2 = \Sigma_{yy} - \Sigma_{zz}$ is simply due to absence of shear in the planes parallel to Oxz. Indeed, particle interactions mainly create additional stresses in the Oxy plane, leading to a negative N_2. Theoretical analyses have been conducted in the dilute regime and predict that α_1 and α_2 vary as ϕ^2 and depend on surface roughness or minimum separation (Brady & Morris 1997; Wilson 2005). In the concentrated regime, Stokesian dynamics simulations have been used to infer the whole suspension stress (Singh & Nott 2000; Sierou & Brady 2002). Frictional particle contact are shown to have a major impact on the magnitude of normal-stress differences (Sierou & Brady 2002).

Only a limited number of measurements are available in the literature. Normal stresses are indeed difficult to measure using standard rheological tools but, in addition, happen to become very small for $\phi \lesssim 0.3$. The first experimental measurements of normal-stress differences was performed by Gadala-Maria (1979), who used a parallel plate geometry to measure the linear combination N_1–N_2. However, this geometry is not actually suitable for suspensions since, for a gap wide enough to have a sufficient quantity of suspension between the plates, drainage often occurs at the boundary. Singh & Nott (2003) have also used a parallel plate geometry in which they have modified the boundary conditions by immersing the rotating discs in a pool of suspension to prevent drainage. By combining stress measurements in this parallel-plate geometry with measurements at the wall of a Couette cell, they have been able to infer N_1 and N_2. Both N_1 and N_2 are found to be negative and are increasing functions of the volume fraction, N_1 being about three times smaller than N_2. An alternative method consists of measuring free-surface deflection induced by the anisotropic stresses such as done in the well-known Weisenberg or rod-climbing effect in polymers (Beavers & Joseph 1975). The great advantage of this method is that it provides a direct measurement of a linear combination of α_1 and α_2 (and not of N_1 and N_2), meaning that one avoids the divergence close to the maximum packing fraction. Zarraga *et al.* (2000) were the first to use a rotating rod immersed in a bath of suspension to study normal-stress differences. In the suspension case, the climbing is down instead of up the rod and the linear combination $\alpha_2 + \alpha_1/2$ can be inferred from measurements of the free surface profile. By combining these measurements with parallel-plate measurements, Zarraga *et al.* (2000) have been able to obtain α_1 and α_2. More recently, Boyer *et al.* (2011) have used the same rotating-rod method but with an enhanced profilometry technique. They have shown that a transition seems to occur at $\phi \approx 0.2$ with a strong linear increase of $\alpha_2 + \alpha_1/2$ for $\phi \gtrsim 0.2$.

However, each of these methods provides a linear combination of the two normal-stress coefficients. This thus implies the use of at least two of them to obtain the two coefficients. This may lead to significant errors and may explain the relative scatter of the data (up to a factor of two). In this study, we present a simple and accurate method to measure directly α_2. This method is inspired by experiments for viscoelastic liquids performed by Tanner (1970) who followed a theoretical analysis of Wineman & Pipkin (1966). It relies on the analysis of the free-surface deflection for a flow down a tilted trough and, to the best of the authors' knowledge, has never been used before in the case of suspensions. Accurate measurements of α_2 are obtained and, by comparison

https://doi.org/10.1017/jfm.2011.315 Published online by Cambridge University Press

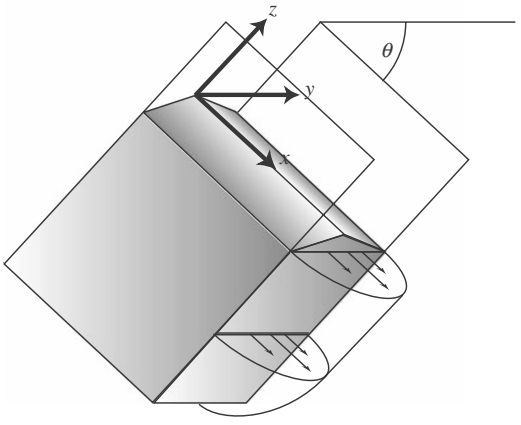


FIGURE 2. Sketch of the tilted-trough flow of a suspension.

with those of Boyer *et al.* (2011) for $\alpha_2 + \alpha_1/2$ with the same batch of particles, estimates of α_1 are given.

This paper is organized as followed. In § 2, a theoretical modelling shows how the free-surface shape is related to the second normal-stress coefficient. The experimental setup and data analysis are described in § 3. Finally, the results are discussed in § 4.

2. Modelling the free-surface profile of the suspension

In this section, we follow the computation presented in § 2.3 (Example 2.3-2) of Bird *et al.* (1987) for interpreting the bulge in the fluid surface which was first described by Wineman & Pipkin (1966) and observed by Tanner (1970) for viscoelastic liquids flowing down a tilted trough. We consider that the trough is very deep so that the presence of the bottom can be ignored, see figure 2. The trough is inclined at an angle θ relatively to the horizontal direction and has a width $2W$. We consider here a suspension as an effective continuous medium. We use a Cartesian coordinate system with origin centred at the middle of the trough and at a level equal to the mean suspension height. The trough (of length L) is supposed to be long enough for the flow to reach steady state.

The existence of the free-surface deflection can be qualitatively understood as follows. Let us consider that the free surface is initially flat. When the trough is inclined, a Poiseuille flow develops in which $\dot{\gamma}$ varies in the y-direction, as shown in figure 2. As $N_2 = \Sigma_{yy} - \Sigma_{zz} \propto \dot{\gamma}$, the magnitude of N_2 is then larger near the wall than in the middle of the trough. Since the surface is initially flat, Σ_{zz} is independent of y. This implies that Σ_{yy} varies along the y-direction. This gradient of transverse stress exerts a net force on the suspension and drives a flow towards the middle, which creates a bulge. This transverse flow stops when the free surface deflection is large enough for the gradient of N_2 to be entirely carried by the gradient of Σ_{zz} (with Σ_{yy} now independent of y). The exact shape of the equilibrium state can then be computed by writing the mass and momentum conservation of the bulk suspension as undertaken in the following.

For small surface deflection, the velocity field is assumed to be purely in the x-direction and to depend only on y

$$\boldsymbol{u} = u_x(y)\boldsymbol{e_x}. \tag{2.1}$$

https://doi.org/10.1017/jfm.2011.315 Published online by Cambridge University Press

We further expect that the shear stress $\tau = |\Sigma_{xy}|$ only depends on y where Σ is the total stress tensor of the suspension.

For Stokesian suspensions of non-Brownian neutrally buoyant spheres (i.e. $Pe \to \infty$ and $Re \to 0$), the shear stress τ is linear in shear rate $|\mathrm{d}u_x/\mathrm{d}y|$

$$\tau = \eta_s(\phi)|\mathrm{d}u_x/\mathrm{d}y|, \tag{2.2}$$

and the second normal-stress difference as well

$$N_2 = \Sigma_{yy} - \Sigma_{zz} = \alpha_2(\phi)\tau. \tag{2.3}$$

Note that the $\alpha_2 = O(1)$ as N_2 and τ are assumed to present the same divergence as ϕ reaches the maximum packing fraction (see e.g. Morris & Boulay 1999; Zarraga *et al.* 2000).

The suspension momentum equations yield along x, y and z, respectively,

$$\frac{\mathrm{d}\Sigma_{xy}}{\mathrm{d}y} = -\rho g \sin\theta \quad \text{leading to } \tau = \rho g|y| \sin\theta, \tag{2.4a}$$

$$\frac{\partial \Sigma_{yy}}{\partial y} = 0 \quad \text{leading to } \frac{\partial(\Sigma_{zz} + N_2)}{\partial y} = 0, \tag{2.4b}$$

$$\frac{\partial \Sigma_{zz}}{\partial z} = \rho g \cos\theta, \tag{2.4c}$$

where $\rho = \rho_p = \rho_f$ for the neutrally buoyant suspensions considered here.

Combining the above equation (2.4*a*) with the constitutive equation (2.3), the second normal-stress difference N_2 is thus given by

$$N_2(y) = \alpha_2 \rho g|y| \sin\theta. \tag{2.5}$$

Integration of (2.4*c*) from the free-surface location $h(y)$ to z gives

$$\Sigma_{zz}(y, z) = -\rho g \cos\theta[h(y) - z] + \gamma\mathscr{C}, \tag{2.6}$$

when taking the jump in normal stress due to the surface tension γ of the suspension into consideration and the atmospheric pressure as reference and where the curvature $\mathscr{C}$ of the free surface is defined as

$$\mathscr{C} = \frac{\dfrac{\mathrm{d}^2 h}{\mathrm{d}^2 y}}{\left[1 + \left(\dfrac{\mathrm{d}h}{\mathrm{d}y}\right)^2\right]^{3/2}}. \tag{2.7}$$

Integration of (2.4*b*) from y to 0, with the use of the two above equations (2.5) and (2.6) as well as of $\mathrm{d}h/\mathrm{d}y = 0$ at $y = 0$ (by taking advantage of the axial symmetry of the problem), leads to

$$h(y) - \frac{\gamma}{\rho g \cos\theta}[\mathscr{C}(y) - \mathscr{C}(0)] = h(0) + \alpha_2|y| \tan\theta. \tag{2.8}$$

Note that $h(0)$ is a constant that can be determined by applying the mass conservation equation, i.e. $\int_{-W}^{W} h(y)\,\mathrm{d}y \equiv 0$.

In the absence of surface tension, the free surface presents a triangular shape (dashed line in figure 3)

$$h(y) = h(0) + |y|\mathscr{S}, \tag{2.9}$$

https://doi.org/10.1017/jfm.2011.315 Published online by Cambridge University Press

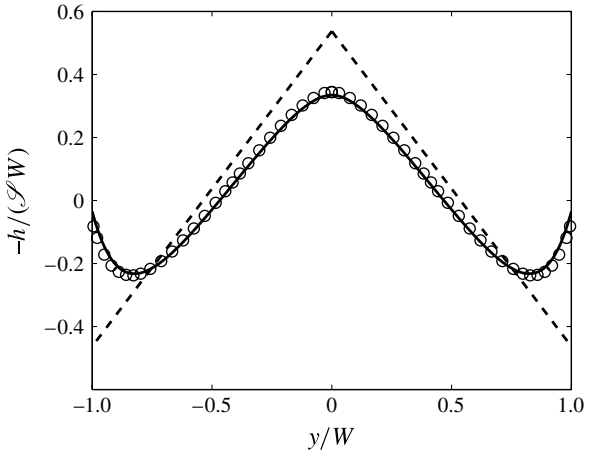


FIGURE 3. Dimensionless surface deflection $-h/\mathscr{S}W$ versus dimensionless radial coordinate y/W with $Bo = 60$, $\beta = 60°$ and $\mathscr{S} = -0.2$: ($\circ$) numerical solution of (2.10), (solid line) analytical solution given by (2.15) and (dashed line) zero-surface-tension solution given by (2.9).

with a slope $\mathscr{S} = \alpha_2 \tan\theta$ which depends both on the volume fraction ϕ and on the tilt angle θ. A negative α_2 leads to a convex shape, as shown in figure 3. Note that the free-surface shape differs from that observed in polymeric liquids flowing down a tilted trough (a convex parabolic bulge) as the normal-stress differences are linear in shear rate modulus $\dot{\gamma}$ for these non-Brownian suspensions whereas they are quadratic in $\dot{\gamma}$ for polymeric liquids (Wineman & Pipkin 1966; Tanner 1970).

When surface tension is taken into account, it is useful to recast (2.8) in dimensionless form by defining $\hat{y} = y/W$ and $\hat{h} = h/\mathscr{S}W$,

$$\hat{h} - \frac{1}{Bo}\frac{\dfrac{\mathrm{d}^2\hat{h}}{\mathrm{d}\hat{y}^2}}{\left[1 + \mathscr{S}^2\left(\dfrac{\mathrm{d}\hat{h}}{\mathrm{d}\hat{y}}\right)^2\right]^{3/2}} = \hat{h}_0 + |\hat{y}| \tag{2.10}$$

where $Bo = \rho g W^2 \cos\theta/\gamma$ is the Bond number and $\hat{h}_0$ the dimensionless constant

$$\hat{h}_0 = \left[\hat{h}(0) - \frac{1}{Bo}\frac{\mathrm{d}^2\hat{h}}{\mathrm{d}\hat{y}^2}(0)\right]. \tag{2.11}$$

Equation (2.10) can be solved numerically with the two boundary conditions

$$\frac{\mathrm{d}\hat{h}}{\mathrm{d}\hat{y}}(1) = \frac{\cot\beta}{\mathscr{S}} \quad \text{and} \quad \frac{\mathrm{d}\hat{h}}{\mathrm{d}\hat{y}}(0) = 0 \tag{2.12}$$

where β is the contact angle at the sidewall.

For small deformation, $\mathscr{S}^2 = (\alpha_2 \tan\theta)^2 \ll 1$, the curvature can be approximated by

$$\mathscr{C} \approx \frac{\mathrm{d}^2 h}{\mathrm{d}^2 y}. \tag{2.13}$$

https://doi.org/10.1017/jfm.2011.315 Published online by Cambridge University Press

This leads to dropping the nonlinear term inside the bracket of (2.10) which then becomes

$$\hat{h} - \frac{1}{Bo}\frac{\mathrm{d}^2\hat{h}}{\mathrm{d}\hat{y}^2} = \hat{h}_0 + |\hat{y}|. \tag{2.14}$$

An analytical solution can be obtained

$$\hat{h} = \hat{h}_0 + \hat{h}_1 + \frac{\cot\beta}{\mathscr{S}}\hat{h}_2 \tag{2.15}$$

with $\hat{h}_1$ and $\hat{h}_2$, respectively, given by

$$\hat{h}_1 = |\hat{y}| + \frac{\cosh(\sqrt{Bo}(|\hat{y}| - 1)) - \cosh(\sqrt{Bo}|\hat{y}|)}{\sqrt{Bo}\sinh(\sqrt{Bo})}, \tag{2.16}$$

and

$$\hat{h}_2 = \frac{\cosh(\sqrt{Bo}|\hat{y}|)}{\sqrt{Bo}\sinh(\sqrt{Bo})}. \tag{2.17}$$

The use of mass conservation, i.e. $\int_{-W}^{W} h(y)\,\mathrm{d}y \equiv 0$, leads to infer

$$\hat{h}_0 = -\frac{1}{2} - \frac{\cot\beta}{\mathscr{S}}\frac{1}{Bo}. \tag{2.18}$$

This analytical solution (2.15) agrees well with the numerical solution of the complete (2.10), as illustrated in figure 3. Significant discrepancy is however seen with the triangular-shape solution obtained for zero surface tension for values of Bo, β and $\mathscr{S}$ corresponding to the present experimental conditions (see § 3). Even far from the walls (where surface tension effects are dominant) and from the middle of the trough, these solutions do not match. The zero-surface-tension solution can only be used for relatively wide troughs. In the following § 3, the analytical solution (2.15) is fitted to the experimental data to infer α_2.

3. Experiments

3.1. *Particles and fluid*

The combination of fluid and particles was similar to that used by Boyer *et al.* (2011) where further details can be found. The Newtonian suspending fluid was poly(ethylene glycol-ran-propylene glycol) monobutylether with density closely matched to that of the particles ($\rho_f = 1.051$ g cm^{-3} at 25 °C) and large viscosity ($\eta_f = 2.15$ Pa s). Two batches of polystyrene spheres having the same density $\rho_p = 1.049 \pm 0.003$ g cm^{-3} but two different radii were used. These spheres had a typical surface roughness height of 0.2 μm as experimentally measured by Boyer *et al.* (2011). The largest spheres had a radius $a = 70 \pm 3$ μm (similar to one of the two batches used by Boyer *et al.* 2011) while the smaller spheres had a radius $a = 35 \pm 5$ μm. The Stokes velocity $(=(2/9)(\rho_p - \rho_f)ga^2/\eta_f)$ was 0.04 mm h^{-1} and 0.01 mm h^{-1} at 25 °C for the two batches, respectively. The sedimentation effect could thus be safely neglected during the experiments that ran over a maximum time scale of 10 min. In addition, the suspension was carefully mixed and let at rest for some time to drive out the remaining air bubbles before each series of experiments. The surface tension γ of the suspension was found equal to that of suspending fluid $\gamma_f = 35$ mN m^{-1}.

https://doi.org/10.1017/jfm.2011.315 Published online by Cambridge University Press

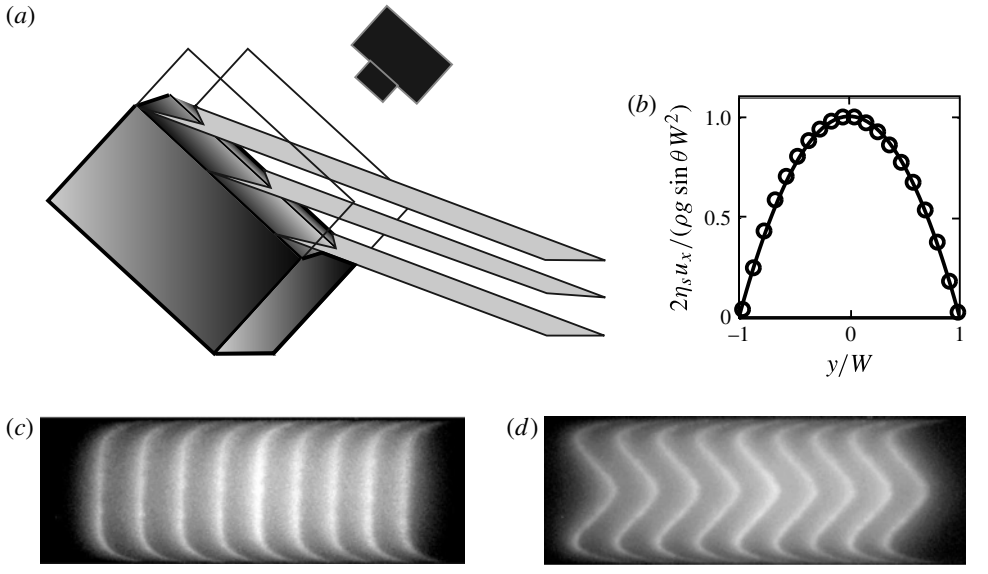


FIGURE 4. (*a*) Sketch of the tilted-trough setup and optical profilometry using laser sheets, (*b*) surface velocity profile (PIV data (○) and quadratic fit (solid line)) at $\phi = 0.5$ and $\theta = 20°$, and picture of the free surface at $\phi = 0.5$ for (*c*) $\theta = 0°$ (at rest) and (*d*) at $\theta = 21°$, for the smallest spheres (see also the accompanying supplementary movie available at journals.cambridge.org/flm).

3.2. *The tilted-trough flow and optical profilometry*

The experimental setup consisted of a parallel-sided channel made of Perspex with a width $2W = 3$ cm, a length $L = 1.60$ m and a suspension-filled height $H = 8$ cm, see figure 4(*a*). The channel was chosen to be long enough for the surface deflection profile to reach a steady state (see the next section). The width was taken not too large to avoid using a large quantity of suspension mixture while maintaining a large height-to-width aspect ratio. This deep trough could be tilted at an angle θ (from 0° to 42°) to the horizontal in order to induce the suspension flow. Using particle image velocimetry (PIV) for particles located on the top layer of the suspension (i.e. at the free surface), we checked that the flow at the surface was a Poiseuille flow, as evidenced in figure 4(*b*). We also verified that the trough was deep enough for the flow to be independent of z. Similar results were indeed obtained with a smaller height of $H = 6$ cm.

The free-surface deflection was measured by optical profilometry in the middle section of the trough. A laser diode equipped with a special head and located at a distance of 70 cm projected a set of 9 quasi-parallel laser sheets onto the surface of the suspension at a fixed angle of ≈8.5°, see figure 4(*a*). A digital camera positioned 35 cm above the channel captured the images of the free surface, see figure 4(*c,d*). Since the local deviation of each line was proportional to the vertical displacement of the free surface, nine surface profiles could be computed by processing the images with a line-tracking technique. The optical calibration was achieved by recording images of a test groove positioned at the location of the free surface. Figure 4 shows typical images of the surface of the suspension at rest (*c*) and when the flow has been induced by tilting the channel at an angle $\theta = 20°$ to the horizontal (*d*), see also the corresponding supplementary movie. The experimental accuracy was found to

https://doi.org/10.1017/jfm.2011.315 Published online by Cambridge University Press

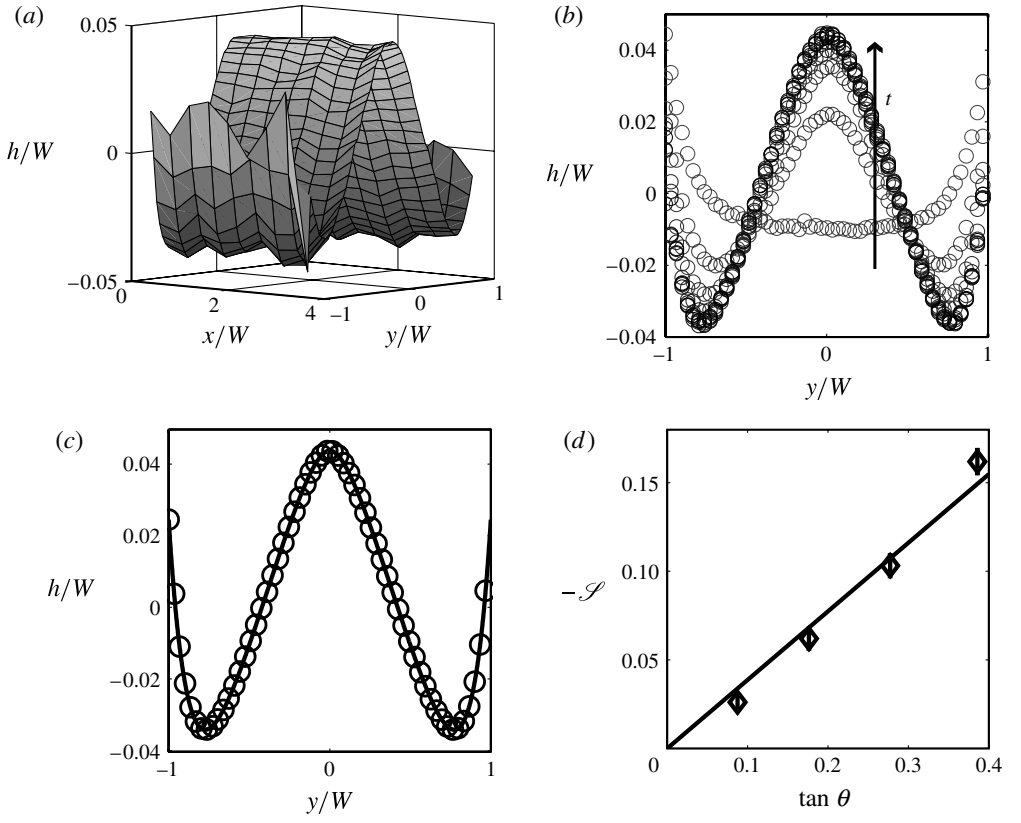


FIGURE 5. (*a*) Reconstruction of the surface profile from the nine surface deflection profiles, (*b*) time-evolution of the average of the nine profiles showing accumulation of data at steady state, (*c*) time-and-space averaged profile (○) and fitted solution given by (3.1) (solid line), and (d) $-\mathscr{S}$ versus $\tan\theta$ (◇) and linear fit (solid line).

be $\Delta h \approx 0.1$ mm (≈one particle diameter) which corresponds to $\rho g \Delta h \approx 1$ Pa. This corresponds also to the smallest signal that can be detected, i.e. the limit of detection.

The Péclet number $Pe = 6\pi\eta_f a^3\dot{\gamma}/kT \simeq 10^9\dot{\gamma}$ was always very large and the particle Reynolds number $Re_p = \rho_p a^2\dot{\gamma}/\eta_f$ very small even for the maximum shear rate ≈50 s^{-1}. The Bond number was $Bo = \rho g W^2 \cos\theta/\gamma \approx 44$–$64$.

It is known that a suspension of non-Brownian particles can exhibit particle migration when submitted to a heterogeneous shear. In a tilted trough of width $2W$, the typical strain leading to migration is given by $(W/a)^2$ (Leighton & Acrivos 1987; Morris & Boulay 1999). In the experiments, the largest strain attained is ≈10 (i.e. much smaller than $(W/a)^2 \simeq 10^4$), thus ensuring that migration can be neglected.

3.3. *Data analysis*

As shown in figure 5(*a*), nine surface deflection profiles can be extracted from the optical profilometry technique as explained above. They are seen to be spatially homogeneous and thus can be averaged. This spatial average over nine profiles is observed to change with time and to reach a saturated shape as evidenced in figure 5(*b*). When a steady state is achieved, a time average can then be performed leading to a time-and-space averaged profile as shown in figure 5(*c*). To compare

https://doi.org/10.1017/jfm.2011.315 Published online by Cambridge University Press

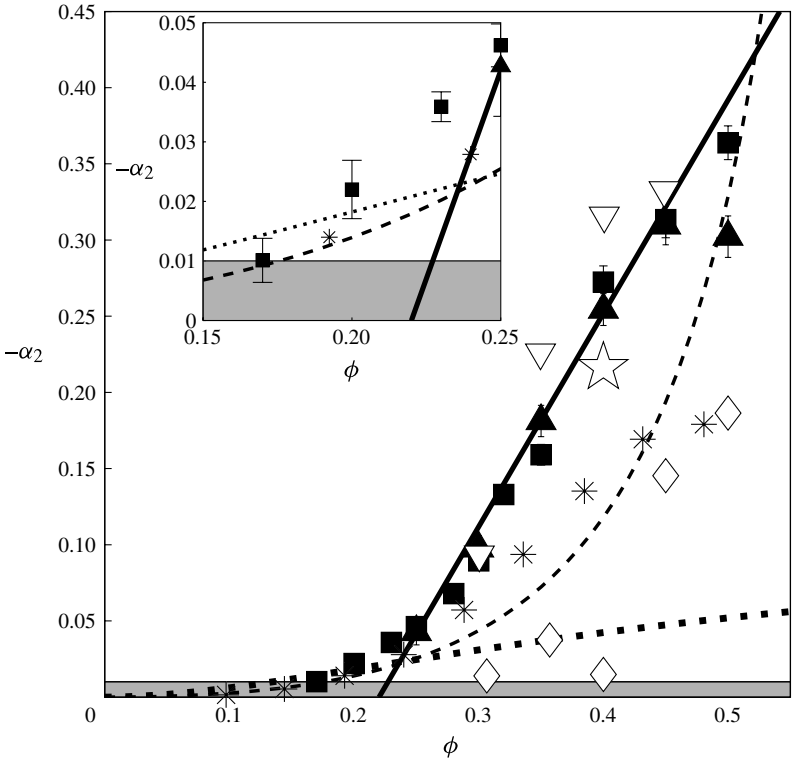


FIGURE 6. Second normal-stress coefficient $-\alpha_2$ versus ϕ. Present experiments: $a = 35 \pm 5$ μm (■) and $a = 70 \pm 5$ μm (▲). Previous experiments: Zarraga *et al.* (2000) (◇), Singh & Nott (2003) (▽). Stokesian dynamics simulations: Sierou & Brady (2002) (∗) without sliding friction and (white star) with a friction coefficient of 0.5. Correlation: Morris & Boulay (1999) (dashed line). Linear fit of Boyer *et al.* (2011): $1.4(\phi–\phi_c)$ (solid line). Inset: blow-up for low ϕ and comparisons with the simulations of Sierou & Brady (2002) without friction (∗), and the analytical calculations of Wilson (2005) with a roughness height of 0.2 μm (dotted line), the correlation of Morris & Boulay (1999) (dashed line). The limit of detection is indicated in grey.

with the analytical solution (2.15) which satisfies mass conservation, the average of the profile across the width is subtracted from the full profile signal. A method of weighted linear least squares (Press *et al.* 2007) is then used to fit the measured signal to the analytical solution (2.15) that we conveniently recast in the form

$$\frac{h}{W} = \left(\hat{h}_1 - \frac{1}{2}\right)\mathscr{S} + \left(\hat{h}_2 - \frac{1}{Bo}\right)\cot\beta, \tag{3.1}$$

exhibiting the two basis functions $\hat{h}_1 - 1/2$ and $\hat{h}_2 - 1/Bo$, see figure 5(*c*). This leads to inferring $-\mathscr{S}$ and its standard variation. The fitting procedure also provides the contact angle β which is not seen to vary significantly from its value at rest, $\beta = 56 \pm 5°$. Note also that the value of surface tension γ is not used as a fitting parameter and is taken equal to the measured value $\gamma = \gamma_f = 35$ mN m^{-1}. The accuracy of this measurement is not critical for the rest of the data analysis: indeed, allowing a 15 % error on the value of γ would lead to an error in α_2 (or $\mathscr{S}$) smaller than the standard deviation (see the error bars in figures 6 and 7). Figure 5(*d*)

https://doi.org/10.1017/jfm.2011.315 Published online by Cambridge University Press

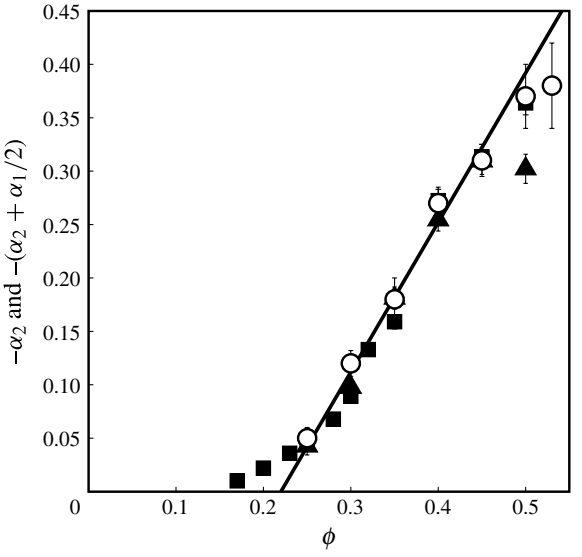


FIGURE 7. Second normal-stress coefficient $-\alpha_2$ versus ϕ for present experiments: $a = 35 \pm 5$ μm (■) and $a = 70 \pm 5$ μm (▲). Normal-stress coefficient combination $-(\alpha_2 + \alpha_1/2)$ versus ϕ for previous experiments of Boyer *et al.* (2011): $a = 70 \pm 5$ μm (○). Linear fit of Boyer *et al.* (2011): $1.4(\phi–\phi_c)$ (solid line).

demonstrates that $-\mathscr{S}$ is linear in $\tan\theta$, as expected from the theoretical analysis of § 2, i.e. $\mathscr{S} = \alpha_2 \tan\theta$. A linear fit using the method of weighted least-squares gives the slope $-\alpha_2$ as well as its standard variation.

4. Discussion

The variation of $-\alpha_2$ with ϕ is shown in figure 6. The data coming from the two batches of particles (■ and ▲) collapse on the same line, thus showing no dependence in particle size, except at the highest volume fraction investigated of $\phi = 0.5$ where $-\alpha_2$ is found smaller for the suspension of the largest spheres. Note that the time to drive out the air bubbles when preparing the suspension considerably increases at this high concentration so that sedimentation could have occurred in the suspension of the largest spheres. Clearly two regimes can be seen. For $\phi < 0.25$, $-\alpha_2$ presents a slow increase with increasing ϕ while for $\phi \gtrsim 0.25$ the increase is stronger and seems to be linear and well represented by the correlation $1.4(\phi–\phi_c)$ (solid line) with $\phi_c = 0.22$ proposed by Boyer *et al.* (2011). No normal-stress differences can be detected for $\phi < 0.17$ within the limit of resolution of the measurement (typically 1 Pa).

The overall increase of $-\alpha_2$ with increasing ϕ is similar to that found in the previous experiments of Zarraga *et al.* (2000) (◇) and Singh & Nott (2003) (▽) and Stokesian dynamics simulations (Sierou & Brady 2002) (∗), although there can be a factor of order two or more between the different data. Note that no normal stresses were reported in the previous experiments for $\phi \leqslant 0.3$ while normal stresses were observed for ϕ as low as 0.1 in the simulations. For $\phi < 0.25$, see inset of figure 6, the present data are of the same order of magnitude than the numerical predictions of Sierou & Brady (2002) (∗) and the analytical predictions of Wilson (2005) (dotted line) taking a roughness height of 0.2 μm as experimentally measured. For $\phi \gtrsim 0.25$, see figure 6, the present data for polystyrene spheres (■ and ▲) lie between the data

https://doi.org/10.1017/jfm.2011.315 Published online by Cambridge University Press

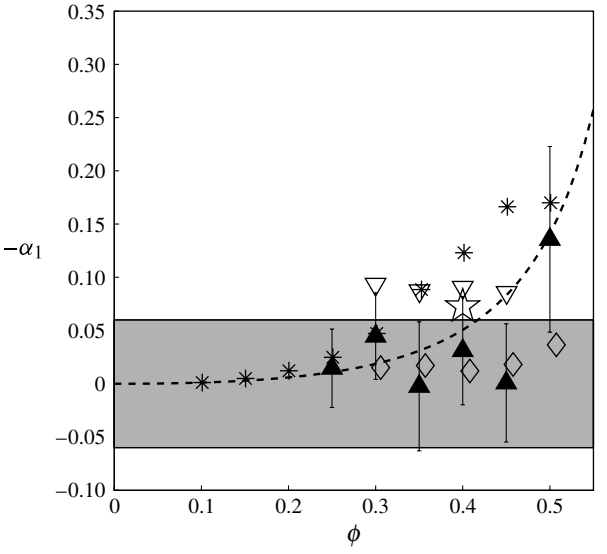


FIGURE 8. First normal-stress coefficient $-\alpha_1$ versus ϕ. Combination of the present experiments and those of Boyer *et al.* (2011), $a = 70 \pm 5$ μm (▲). Previous experiments, Zarraga *et al.* (2000) (◇), Singh & Nott (2003) (▽). Stokesian dynamics simulations: Sierou & Brady (2002) (∗) without sliding friction and (white star) with a friction coefficient of 0.5. Correlation: Morris & Boulay (1999) (dashed line). The accuracy is indicated in grey.

of Zarraga *et al.* (2000) for glass spheres (◇) and Singh & Nott (2003) for polymethyl methacrylate (PMMA) spheres (▽). They are also always larger than the predictions of the Stokesian dynamics simulations (Sierou & Brady 2002) without sliding friction between the particles (∗). Good agreement is obtained when the effect of friction is included in the simulations (white star for $\phi = 0.40$ with a friction coefficient of 0.5). The simple linear increase (solid line) proposed by Boyer *et al.* (2011) seems to better match the data than the correlation of Morris & Boulay (1999).

Figure 7 shows, in the same plot, both the present data for $-\alpha_2$ (■ and ▲) and those of Boyer *et al.* (2011) for $-(\alpha_2 + \alpha_1/2)$ (○). Interestingly, there is no detectable difference within error bars between these two measurements. The deduced $-\alpha_1$ for the same batch of particles used here and in Boyer *et al.* (2011) is plotted versus ϕ in figure 8. It fluctuates around zero and one cannot tell whether it is positive or negative, i.e. $-0.06 \lesssim \alpha_1 \lesssim 0.06$ (except for $\phi = 0.5$ for which it seems to be positive). The previous experiments of Zarraga *et al.* (2000) (◇) and Singh & Nott (2003) (▽) also found very small values of $-\alpha_1$, but they seem to be positive (meaning α_1 negative). Larger $-\alpha_1$ are obtained in the Stokesian dynamics simulations (Sierou & Brady 2002) without sliding friction between the particles (∗). Adding friction leads to smaller $-\alpha_1$ (white star with a friction coefficient of 0.5).

5. Conclusion

In summary, we have used a method for finding the second normal-stress difference of suspensions which relies on the examination of the shape of the suspension free surface in a tilted trough flow (Wineman & Pipkin 1966; Tanner 1970). The second normal-stress difference is negative and is linear in shear stress. The absolute value of the ratio of the second normal-stress difference to shear stress, also called second

https://doi.org/10.1017/jfm.2011.315 Published online by Cambridge University Press

normal-stress difference coefficient, increases with increasing volume fraction. A clear behavioural change in this coefficient exhibiting a strong (linear) growth with volume fraction is seen above a volume fraction of 0.22. By comparing with previous data obtained for the same batch of spheres by Boyer *et al.* (2011), the first normal-stress difference coefficient can be estimated. Its magnitude is very small ($\lesssim 0.06$) and it is hard to tell whether it is negative, positive or even zero.

The two major outcomes of this study are (i) the transition in behaviour seen for the second normal-stress difference coefficient around a volume fraction of $\phi_c = 0.22$ and (ii) the difference in magnitude observed for the first and second normal-stress differences. The interplay between hydrodynamic and contact (or friction) interactions may be fundamental in explaining these behaviours.

The present results complemented by those of Boyer *et al.* (2011) suggest that $\Sigma_{xx} \approx \Sigma_{yy}$. Together with $\Sigma_{zz} = \Sigma_{xx}/2$ given by the lack of migration in parallel plate geometry (Morris & Boulay 1999), this leads to

$$\Sigma_{xx} \approx \Sigma_{yy} = -g(\phi)\tau, \tag{5.1a}$$

$$\Sigma_{zz} = -\tfrac{1}{2}g(\phi)\tau, \tag{5.1b}$$

with $g(\phi) = -2\alpha_2(\phi)$ a function of concentration provided by the data of figure 6 which present a growth approximately linear in ϕ–ϕ_c for $0.5 \gtrsim \phi \gtrsim \phi_c$, and provides a full phenomenological form for the normal stresses of suspensions.

Funding from Agence Nationale de la Recherche (Project RSC ANR-08-BLAN-0048-CSD2) is gratefully acknowledged.

Supplementary movies are available at journals.cambridge.org/flm.

REFERENCES

ARP, A. P. & MASON, S. G. 1977 The kinetics of flowing dispersions. IX. Doublets of rigid spheres (experimental). *J. Colloid Interface Sci.* **61**, 44–61.

BATCHELOR, G. K. & GREEN, J. T. 1972 The determination of the bulk stress in a suspension of spherical particles to order c^2. *J. Fluid Mech.* **56**, 401–427.

BEAVERS, G. S. & JOSEPH, D. D. 1975 The rotating-rod viscometer. *J. Fluid Mech.* **69**, 475–512.

BIRD, R. B., ARMSTRONG, R. C. & HASSAGER, O. 1987 *Dynamics of Polymeric Liquids*, 2nd edn. *Fluid Dynamics*, vol. 1. John Wiley & Sons.

BOYER, F., POULIQUEN, O. & GUAZZELLI, E. 2011 Dense suspensions in rotating-rod flows: normal stresses and particle migration. *J. Fluid Mech.* **686**, 5–25.

BRADY, J. F & CARPEN, I. C. 2001 Second normal stress jump instability in non-Newtonian fluids. *J. Non-Newtonian Fluid Mech.* **2075**, 1–14.

BRADY, J. F & MORRIS, J. F. 1997 Microstructure of strongly sheared suspensions and its impact on rheology and diffusion. *J. Fluid Mech.* **348**, 103–139.

DAVIS, R. H. 1992 Effects of surface roughness on a sphere sedimenting through a dilute suspension of neutrally buoyant spheres. *Phys. Fluids* A **4**, 2607–2619.

GADALA-MARIA, F. 1979 The rheology of concentrated suspensions. PhD thesis, Stanford University.

LEIGHTON, D. T. & ACRIVOS, A. 1987 The shear-induced migration of particles in concentrated suspensions. *J. Fluid Mech.* **181**, 415–439.

MORRIS, J. F. & BOULAY, F. 1999 Curvilinear flows of non-colloidal suspensions: the role of normal stresses. *J. Rheol.* **43**, 1213–1237.

PARSI, F. & GADALA-MARIA, F. 1987 Fore-and-aft asymmetry in a concentrated suspension of solid spheres. *J. Rheol.* **31**, 725–732.

PRESS, W. H., TEUKOLSKY, S. A., FLANNERY, B. , P. & VETTERLING, W. T. 2007 *Numerical Recipes: The Art of Scientific Computing*, 3rd edn. Cambridge University Press.

https://doi.org/10.1017/jfm.2011.315 Published online by Cambridge University Press

RAMACHANDRAN, A. & LEIGHTON, D. T. 2008 The influence of secondary flows induced by normal stress differences on the shear-induced migration of particles in concentrated suspensions. *J. Fluid Mech.* **603**, 207–243.

RAMPALL, I., SMART, J. R. & LEIGHTON, D. T. 1997 The influence of surface roughness on the particle-pair distribution function of dilute suspensions of non-colloidal spheres in simple shear flow. *J. Fluid Mech.* **339**, 1–24.

SIEROU, A. & BRADY, J. F. 2002 Rheology and microstructure in concentrated non-colloidal suspensions. *J. Rheol.* **46**, 1031–1056.

SINGH, A. & NOTT, P. R. 2000 Normal stresses and microstructure in bounded sheared suspensions via Stokesian dynamics simulations. *J. Fluid Mech.* **412**, 279–301.

SINGH, A. & NOTT, P. R. 2003 Experimental measurements of the normal stresses in sheared Stokesian suspensions. *J. Fluid Mech.* **490**, 293–320.

STICKEL, J. J. & POWELL, R. L. 2005 Fluid mechanics and rheology of dense suspensions. *Annu. Rev. Fluid Mech.* **37**, 129–149.

TANNER, R. I. 1970 Some methods for estimating the normal stress functions in viscometric flows. *Trans. Soc. Rheol.* **14** (4), 483–507.

WILSON, H. J. 2005 An analytic form for the pair distribution function and rheology of a dilute suspension of rough spheres in plane strain flow. *J. Fluid Mech.* **534**, 97–114.

WINEMAN, A. & PIPKIN, A. 1966 Slow viscoelastic flow in tilted troughs. *Acta Mechanica* **2**, 104–115.

ZARRAGA, I. E., HILL, D. A. & LEIGHTON, D. T. 2000 The characterization of the total stress of concentrated suspensions of non-colloidal spheres in Newtonian fluids. *J. Rheol.* **44**, 185–220.

https://doi.org/10.1017/jfm.2011.315 Published online by Cambridge University Press